



Observation of the $B^+ \rightarrow J/\psi\eta'K^+$ decay

LHCb collaboration

Abstract

The $B^+ \rightarrow J/\psi\eta'K^+$ decay is observed for the first time using proton-proton collision data collected by the LHCb experiment at centre-of-mass energies of 7, 8, and 13 TeV, corresponding to a total integrated luminosity of 9 fb^{-1} . The branching fraction of this decay is measured relative to the known branching fraction of the $B^+ \rightarrow \psi(2S)K^+$ decays and found to be

$$\frac{\mathcal{B}(B^+ \rightarrow J/\psi\eta'K^+)}{\mathcal{B}(B^+ \rightarrow \psi(2S)K^+)} = (4.91 \pm 0.47 \pm 0.29 \pm 0.07) \times 10^{-2},$$

where the first uncertainty is statistical, the second is systematic and the third is related to external branching fractions. A first look at the $J/\psi\eta'$ mass distribution is performed and no signal of intermediate resonances is observed.

Submitted to JHEP

1 Introduction

In the last twenty years a plethora of new hadron states have been discovered in decays of beauty hadrons to charmonia, including the enigmatic $\chi_{c1}(3872)$ state [1], numerous pentaquark states in $J/\psi p$ [2–6] and $J/\psi \Lambda$ [7] systems as well as tetraquarks in the $\psi(2S)\pi^+$ [8–12], $J/\psi \phi$ [13–17], $\eta_c(1S)\pi^-$ [18], $J/\psi\pi^+$ [19], $J/\psi K^+$ [16] and $J/\psi K_S^0$ [17] systems. Transitions among charmonia or charmonia-like states have been studied in beauty-hadron decays, including transitions with emission of one photon [20–23], two pions [24–27], ϕ [13–17], ω [27, 28] and η [29] mesons. The transitions with emission of an η meson have also been studied in $e^+e^- \rightarrow J/\psi\eta$ processes [30, 31]. In general, studies of various hadronic transitions in the charmonia and charmonia-like sectors can shed light into the internal structure of these particles, which is largely unknown for newly discovered hadronic states [32–35].

Transitions with an emission of an η' meson in the charmonia and charmonia-like systems have not yet been observed [32, 36, 37]. Since the η' meson may have a glueball contribution [38–55], processes involving this particle are of particular interest [56, 57]. The $B^+ \rightarrow J/\psi\eta'K^+$ decay¹ is a good candidate to explore the $J/\psi\eta'$ system in detail, offering the opportunity to search for possible intermediate resonances. The decay itself has never been observed and an upper limit on its branching fraction of

$$\mathcal{B}(B^+ \rightarrow J/\psi\eta'K^+) < 8.8 \times 10^{-5} \text{ (90\% CL)},$$

was set by the Belle collaboration [58].

This paper reports the observation of the $B^+ \rightarrow J/\psi\eta'K^+$ decay using proton-proton (pp) collision data collected by the LHCb experiment at centre-of-mass energies of 7, 8, and 13 TeV, corresponding to a total integrated luminosity of 9 fb^{-1} . The measurement of its branching fraction normalised to the well-known branching fraction of the $B^+ \rightarrow \psi(2S)K^+$ decay [37],

$$\mathcal{R} \equiv \frac{\mathcal{B}(B^+ \rightarrow J/\psi\eta'K^+)}{\mathcal{B}(B^+ \rightarrow \psi(2S)K^+)}, \quad (1)$$

is performed using the $\eta' \rightarrow \rho^0\gamma$ decay. The observation of the signal is confirmed using the $\eta' \rightarrow \eta\pi^+\pi^-$ decay mode, which is also used as a cross-check.

2 Detector and simulation

The LHCb detector [59, 60] is a single-arm forward spectrometer covering the pseudorapidity range $2 < \eta < 5$, designed for the study of particles containing b or c quarks. The detector includes a high-precision tracking system consisting of a silicon-strip vertex detector surrounding the pp interaction region [61], a large-area silicon-strip detector located upstream of a dipole magnet with a bending power of about 4 Tm, and three stations of silicon-strip detectors and straw drift tubes [62, 63] placed downstream of the magnet. The tracking system provides a measurement of the momentum, p , of charged particles with a relative uncertainty that varies from 0.5% at low momentum to 1.0% at 200 GeV/ c . The minimum distance of a track to a primary pp collision vertex (PV),

¹Inclusion of charge-conjugate states is implied throughout the paper, unless otherwise stated.

the impact parameter is measured with a resolution of $(15 + 29/p_T)$ μm , where p_T is the component of the momentum transverse to the beam, in GeV/c . Different types of charged hadrons are distinguished using information from two ring-imaging Cherenkov detectors [64]. Photons, electrons and hadrons are identified by a calorimeter system consisting of scintillating-pad and preshower detectors, an electromagnetic and a hadronic calorimeter. Muons are identified by a system composed of alternating layers of iron and multiwire proportional chambers [65].

The online event selection is performed by a trigger [66,67], which consists of a hardware stage, based on information from the calorimeter and muon systems, followed by a software stage, which applies a full event reconstruction. At the hardware trigger stage, events are required to have a muon track with high transverse momentum or dimuon candidates in which the product of the p_T of the muons has a high value. In the software trigger, two oppositely charged muons are required to form a good-quality vertex that is significantly displaced from every PV, with a dimuon mass exceeding $2.7 \text{ GeV}/c^2$.

Simulated events are used to describe signal shapes and to compute the efficiencies needed to determine the branching fraction ratio. In the simulation, pp collisions are generated using PYTHIA [68] with a specific LHCb configuration [69]. Decays of unstable particles are described by EVTGEN [70], in which final-state radiation is generated using PHOTOS [71]. The interaction of the generated particles with the detector, and its response, are implemented using the GEANT4 toolkit [72] as described in Ref. [73]. The p_T and rapidity (y) spectra of the B^+ mesons in simulation are corrected to match distributions in data. The correction factors are calculated by comparing the observed p_T and y spectra for a high-purity data sample of reconstructed $B^+ \rightarrow J/\psi K^+$ decays with the corresponding simulated samples. In the simulation, the $B^+ \rightarrow J/\psi \eta' K^+$ decays are generated as phase-space decays and corrected using a gradient boosted decision tree reweighting algorithm [74] to reproduce the $J/\psi \eta'$ and $\eta' K^+$ mass spectra observed in data. To describe accurately the variables used for kaon identification, the corresponding quantities in simulation are resampled according to values obtained from calibration data samples of $D^{*+} \rightarrow (D^0 \rightarrow K^- \pi^+) \pi^+$ decays [75]. The procedure accounts for correlations between the variables associated to a particular track, as well as the dependence of the kaon identification response on the track's p_T and η and the multiplicity of tracks in the event. To account for imperfections in the simulation of charged-particle reconstruction, the track reconstruction efficiency is corrected using a sample of $J/\psi \rightarrow \mu^+ \mu^-$ decays in data [76]. Samples of the $B^+ \rightarrow J/\psi K^{*+}$ decays with $K^{*+} \rightarrow K^+ (\pi^0 \rightarrow \gamma\gamma)$ are used to correct the photon reconstruction efficiency in simulation [77–80].

3 Event selection

The $B^+ \rightarrow J/\psi \eta' K^+$ candidates are reconstructed with η' decays to both $(\rho^0 \rightarrow \pi^+ \pi^-) \gamma$ or $(\eta \rightarrow \gamma\gamma) \pi^+ \pi^-$ final states. Although the latter has a larger branching fraction, the difficulty of reconstructing photons in the $\eta \rightarrow \gamma\gamma$ decay leads to a sample with fewer events. The $B^+ \rightarrow \psi(2S) K^+$ normalisation decay is reconstructed using the $\psi(2S) \rightarrow J/\psi \pi^+ \pi^-$ decay. In both signal and normalisation channels, the J/ψ meson is reconstructed in its decay to two muons. As explained in detail below, an initial loose selection is applied for both signal and normalisation channels. Subsequently, for the $B^+ \rightarrow J/\psi \eta' K^+$ candidates, where the background level is large, a multivariate estimator is used to select higher

purity subset of candidates. The normalisation channel has a high purity after the initial selection, therefore no further selection steps are applied.

To reduce systematic uncertainties, the initial selection criteria for both signal and normalisation channels are kept the same whenever possible. The selection criteria are chosen to be similar to those used in previous LHCb studies [20, 21, 23, 29, 53, 77, 78]. The muon, pion and kaon candidates are identified by combining information from the Cherenkov detectors, calorimeters and muon detectors [81] associated to the reconstructed tracks. To reduce the combinatorial background, only tracks that are inconsistent with originating from any reconstructed PV in the event are considered. The transverse momentum of the muon candidates is required to be greater than 500 MeV/ c and their momenta must exceed 6 GeV/ c . Pairs of oppositely-charged muons consistent with originating from a common vertex are combined to form $J/\psi \rightarrow \mu^+ \mu^-$ candidates. The reconstructed mass of the muon pair is required to be between 3.056 and 3.136 GeV/ c^2 .

Tracks that are consistent with the pion or kaon hypotheses are required to have transverse momentum greater than 200 MeV/ c . Photons are reconstructed from clusters in the electromagnetic calorimeter, with transverse energy above 350 MeV. The clusters must not be associated with reconstructed tracks [82, 83]. Photon identification is based on the combined information from electromagnetic and hadronic calorimeters, scintillation pad, preshower detectors and the tracking system.

For the reconstruction of the $\eta' \rightarrow \eta \pi^+ \pi^-$ candidates, two photons are first combined to form an η candidate. The diphoton mass is restricted to lie within ± 60 MeV/ c^2 around the known mass of the η meson [37]. Each η candidate is then combined with two oppositely-charged pions to form an η' candidate. The mass of the combination is required to lie within ± 45 MeV/ c^2 around the known mass of the η' meson [37]. For an η' candidate reconstructed in the $\eta' \rightarrow \rho^0 \gamma$ decay mode, the ρ^0 candidate is formed from two oppositely-charged pions. The mass of this candidate is restricted to lie between 500 and 900 MeV/ c^2 . This asymmetric region around the known mass of the ρ^0 meson [37] takes into account the shift of the ρ^0 line shape, due to the electric-dipole nature of the $\eta' \rightarrow \rho^0 \gamma$ transition [84–89]. A photon is combined with the ρ^0 candidate in order to form the η' candidate, whose mass is required to lie within ± 30 MeV/ c^2 of the known η' mass [37].

Each selected J/ψ candidate is combined with a kaon track and either an η' candidate or two oppositely-charged pions to form a B^+ candidate decaying into the signal or normalisation modes, respectively. For the $B^+ \rightarrow \psi(2S)K^+$ candidates the $J/\psi \pi^+ \pi^-$ mass is required to be between 3.66 and 3.71 GeV/ c^2 . To improve the B^+ meson mass resolution a kinematic fit [90] is performed, which constrains the masses of the J/ψ , η' and η candidates to their known values [37], and the B^+ candidates to originate from its associated PV. The decay time of the B^+ candidates is required to be greater than 100 $\mu\text{m}/c$ to suppress the large combinatorial background from tracks created in a PV.

Further selection of the $B^+ \rightarrow J/\psi \eta' K^+$ decays is based on a multivariate estimator, in the following referred to as the multi-layer perceptron (MLP) classifier. The classifier is based on an artificial neural network algorithm [91, 92], configured with a cross-entropy cost estimator [93]. It reduces the combinatorial background to a low level while retaining a high signal efficiency. Two MLP classifiers are trained separately for the two different η' meson decay modes. In both cases the same variables are included in the classifiers and these are related to the reconstruction quality, kinematics and decay time of the B^+ candidates, kinematics of the final-state particles and a variable that characterises the kaon identifi-

cation. The classifiers are trained using simulated samples of $B^+ \rightarrow J/\psi\eta'K^+$ decays as signal proxy, while the $B^+ \rightarrow J/\psi\eta'K^+$ candidates from data with mass above $5.35 \text{ GeV}/c^2$ are used to represent the background. The $B^+ \rightarrow J/\psi(\eta' \rightarrow \rho^0\gamma)K^+$ candidates with the $J/\psi\pi^+\pi^-K^+$ mass within $\pm 21 \text{ MeV}/c^2$ around the known mass of the B^+ meson are vetoed to avoid contamination from the $B^+ \rightarrow J/\psi\pi^+\pi^-K^+$ decays with a random photon added.

The requirement on each of the MLP classifiers is chosen to maximise the figure-of-merit defined as $S/\sqrt{B+S}$, where S represents the expected signal yield, and B is the expected background yield within a $\pm 15 \text{ MeV}/c^2$ mass window centred around the known mass of the B^+ meson. The background yield is calculated from fits to data, while the expected signal yield is estimated as $S = \varepsilon S_0$, where ε is the efficiency of the requirement on the response of the MLP classifier determined from simulation, and S_0 is the signal yield obtained from the fit to the data with a loose requirement applied. The mass distributions for the selected $B^+ \rightarrow J/\psi\eta'K^+$ candidates are shown in Fig. 1, where clear signal peaks corresponding to B^+ decays are seen in data for both η' decay modes.

4 Signal yield determination

The signal yields are determined using an extended unbinned maximum-likelihood fit with a two-component function. The signal component for both cases is modelled by a modified Gaussian function with power-law tails on both sides of the distribution [94,95]. The background component is parameterised by a second-order positive polynomial function [96] for B^+ mesons reconstructed through the $\eta' \rightarrow \rho^0\gamma$ decay mode and by an exponential function in case of the $\eta' \rightarrow \eta\pi^+\pi^-$ decay mode. The tail parameters of the signal components are taken from simulation. The detector resolution is taken from simulation and further corrected by a scale factor, s_{B^+} , that accounts for a small discrepancy between data and simulation [15,26,29,97,98]. To account for the uncertainty in the tail parameters and resolution, the fit is performed simultaneously for data and simulated samples, sharing the same tail parameters, and allowing the correction factor s_{B^+} to vary. The fit results are overlaid in Fig. 1 and the signal yields are found to be

$$N_{B^+ \rightarrow J/\psi\eta'K^+} \Big|_{\eta' \rightarrow \rho^0\gamma} = (1.11 \pm 0.11) \times 10^3, \quad (2a)$$

$$N_{B^+ \rightarrow J/\psi\eta'K^+} \Big|_{\eta' \rightarrow \eta\pi^+\pi^-} = (0.228 \pm 0.028) \times 10^3, \quad (2b)$$

where the uncertainties are statistical only. The resolution correction factors s_{B^+} are found to be 1.08 ± 0.12 and 1.03 ± 0.16 for the $\eta' \rightarrow \rho^0\gamma$ and $\eta' \rightarrow \eta\pi^+\pi^-$ samples, respectively. In both cases, the statistical significance of the $B^+ \rightarrow J/\psi\eta'K^+$ signal is calculated using Wilks' theorem [99] and found to exceed 17 and 12 standard deviations for the $\eta' \rightarrow \rho^0\gamma$ and $\eta' \rightarrow \eta\pi^+\pi^-$ samples, respectively. However, as the signal yield is much lower for the η' meson decays to the $\eta\pi^+\pi^-$ final state, all subsequent studies are performed using only the $\eta' \rightarrow \rho^0\gamma$ decay mode.

The background-subtracted $J/\psi\eta'$, $\eta'K^+$, and $J/\psi K^+$ mass spectra from the $B^+ \rightarrow J/\psi(\eta' \rightarrow \rho^0\gamma)K^+$ decays are shown in Figs. 2(a-c), where the *sPlot* technique [100] based on the fit results is used for background subtraction. The $J/\psi\eta'$, $\eta'K^+$, and $J/\psi K^+$ masses are calculated using a kinematic fit with J/ψ , η' and B^+ mass constraints and a PV constraint applied [90]. While for the $J/\psi K^+$ mass the distribution largely agrees with the shape expected from the phase-space model, for the low-mass

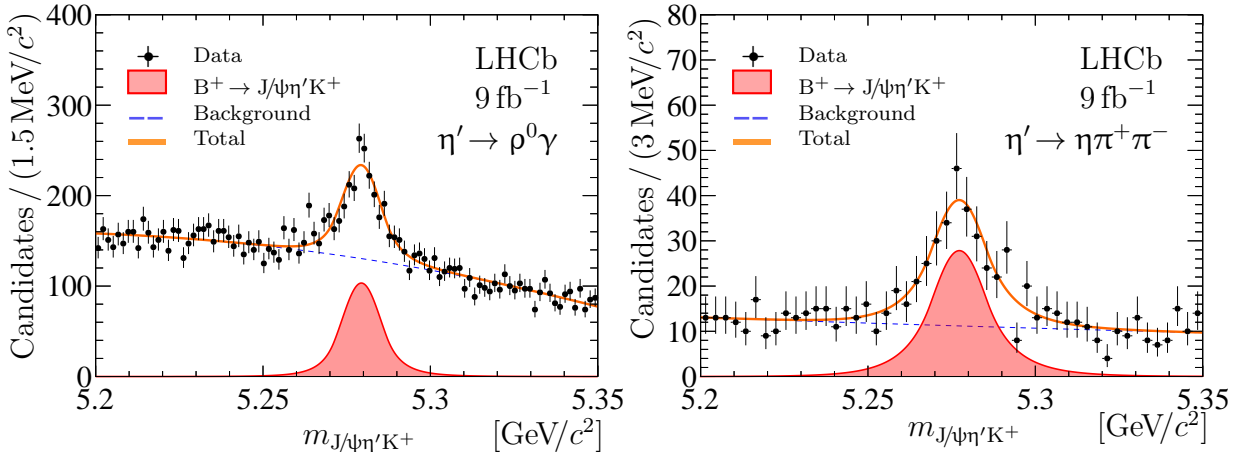


Figure 1: Mass distributions for selected $B^+ \rightarrow J/\psi\eta'K^+$ candidates with η' decays to (left) $\rho^0\gamma$ and (right) $\eta\pi^+\pi^-$ final states. The results of the fits, described in the text, are overlaid.

region of the $\eta'K^+$ mass spectrum and the high-mass region of the $J/\psi\eta'$ mass spectrum a striking difference from the phase-space model is observed. These differences are potentially due to contributions from decays via intermediate heavy excited strange mesons, such as $K_0^*(1430)^+$, $K_2^*(1430)^+$ or $K^*(1680)^+$ mesons, decaying into the $\eta'K^+$ final state. The decays of the B^+ mesons into a J/ψ meson and heavy excited strange mesons have been studied in Refs. [13, 14, 16]. Large contribution from the decays with intermediate excited kaons could also explain the higher mass region of the $J/\psi\eta'$ mass spectrum, as shown in Fig. 2(d).

While the higher mass region of the $J/\psi\eta'$ mass spectrum is presumably dominated by the contributions from the decays via intermediate heavy excited kaons, the $J/\psi\eta'$ mass region below $4.7\text{ GeV}/c^2$ is explicitly inspected for possible contributions from decays via excited charmonia or charmonium-like states into the $J/\psi\eta'$ final state. Fits to the background-subtracted $J/\psi\eta'$ mass distribution are performed in individual mass windows, corresponding to the well-established $\psi(4160)$, $\psi(4230)$, $\psi(3460)$, $\psi(4415)$ and $\psi(4430)$ resonances [37]. For each fit, the resonance shape is parameterised with a relativistic Breit–Wigner function convoluted with a mass resolution function. The non-resonant contribution is modelled by a first order polynomial function. The known masses and widths of the resonances [37] are introduced in the fits as Gaussian constraints on the corresponding parameters. The resolution function is obtained using simulation as a function of the $J/\psi\eta'$ mass. No statistically significant signals are observed for the $B^+ \rightarrow J/\psi\eta'K^+$ decays via intermediate resonances, listed above.

For the determination of the resonant structure of the $B^+ \rightarrow J/\psi\eta'K^+$ decay, a full amplitude analysis, similar to those used in Refs. [14, 16], is required. Large signal yields and low background levels are important prerequisites for such analysis. The relatively large level of combinatorial background for the $B^+ \rightarrow J/\psi\eta'K^+$ signal decays with the η' meson reconstructed via the $\eta' \rightarrow \rho^0\gamma$ decay mode, makes it difficult to carry out an amplitude analysis. With a larger data sample, expected from future data-taking periods, it will be possible to perform the full amplitude analysis using the $B^+ \rightarrow J/\psi\eta'K^+$ signal decays with the η' meson reconstructed via the $\eta' \rightarrow \eta\pi^+\pi^-$ decay mode, where the combinatorial background is smaller.

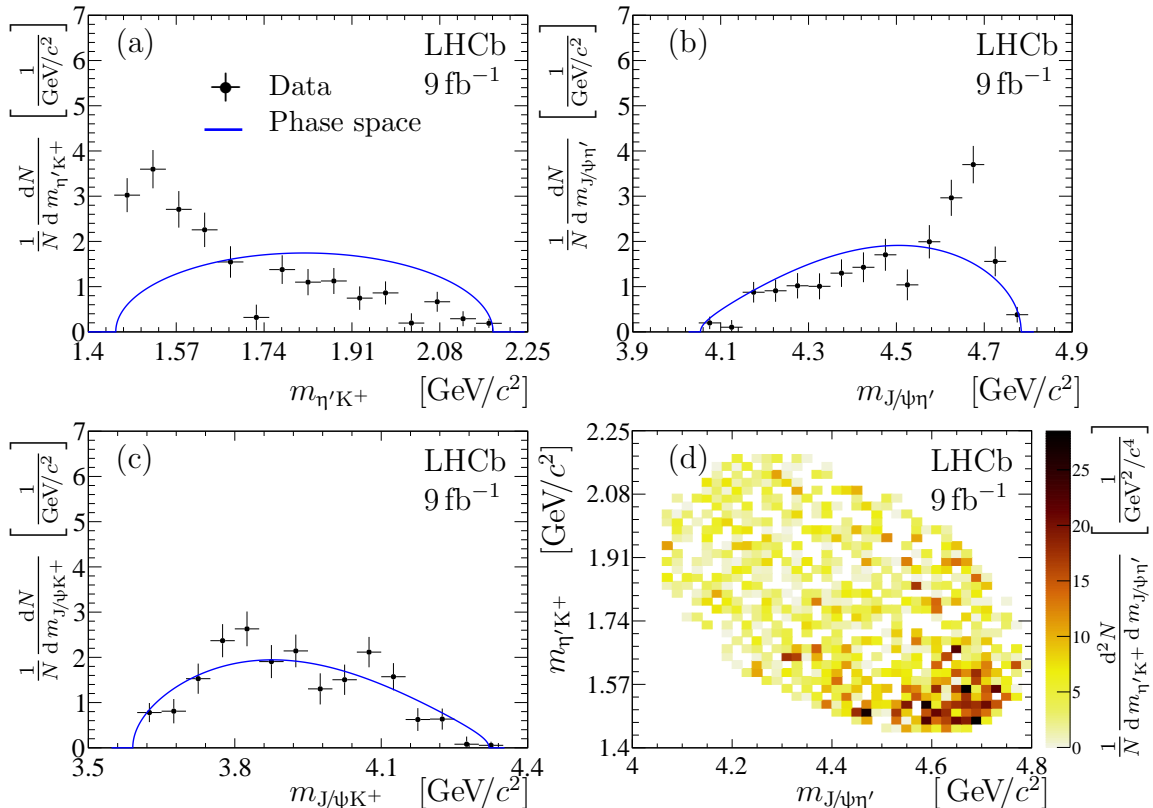


Figure 2: Normalised background-subtracted (a) $\eta'K^+$, (b) $J/\psi\eta'$, (c) $J/\psi K^+$ mass spectra and (d) two-dimensional mass distribution of $\eta'K^+$ vs $J/\psi\eta'$ from the $B^+ \rightarrow J/\psi\eta'K^+$ decays. Superimposed curves are the expectations from a phase-space model.

5 Normalisation channel

The $J/\psi\pi^+\pi^-K^+$ mass distribution for selected $B^+ \rightarrow (\psi(2S) \rightarrow J/\psi\pi^+\pi^-)K^+$ candidates with $J/\psi\pi^+\pi^-$ mass between 3.66 and 3.71 GeV/c^2 is shown in Fig. 3(left). An extended unbinned maximum-likelihood fit is performed, where the signal component is modelled by a modified Gaussian function with power-law tails and the background is described by a first order polynomial function. The result of this fit is used to obtain the background-subtracted $J/\psi\pi^+\pi^-$ mass distribution from $B^+ \rightarrow J/\psi\pi^+\pi^-K^+$ decays. This distribution is shown in Fig. 3(right). The yield of the $B^+ \rightarrow (\psi(2S) \rightarrow J/\psi\pi^+\pi^-)K^+$ signal candidates is determined using an unbinned fit to this distribution with a two-component function. The component corresponding to the $B^+ \rightarrow \psi(2S)K^+$ decays is parameterised by a modified Gaussian function with power-law tails. The component describing the $B^+ \rightarrow J/\psi\pi^+\pi^-K^+$ decays without intermediate $\psi(2S)$ state is modelled by a phase-space function,² modified by a first order polynomial function. The tail and resolution parameters for the signal compo-

²The phase-space mass distribution of a k -body combination of particles from an n -body decay is approximated by $\Phi_{k,n}(x) \propto x_*^{(3k-5)/2} (1-x_*)^{3(n-k)/2-1}$, where $x_* \equiv (x - x_{\min})/(x_{\max} - x_{\min})$, and x_{\min} , x_{\max} denote the minimal and maximal values of x , respectively [101]. Here, $k = 3$ and $n = 4$ are used.

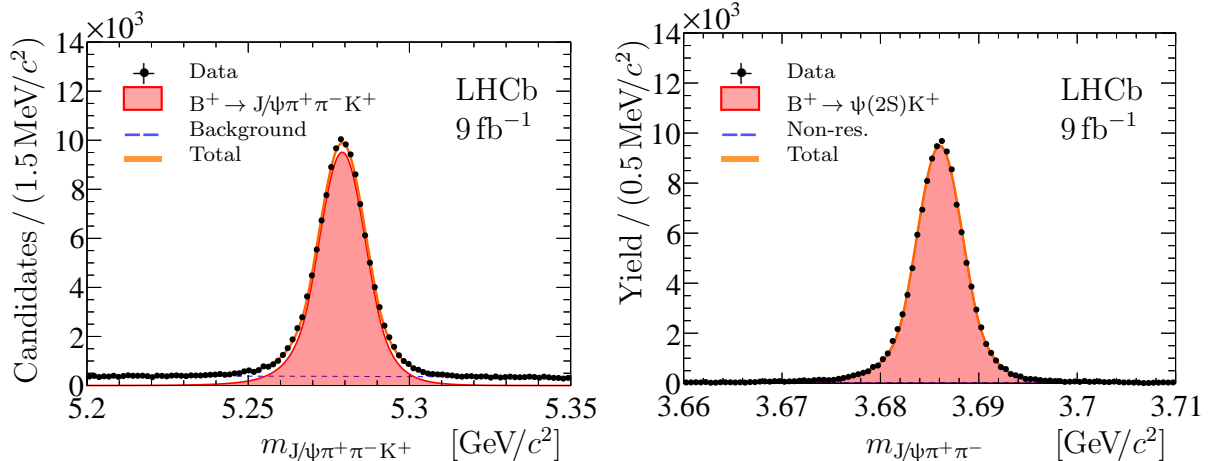


Figure 3: Left: mass distributions for selected $B^+ \rightarrow (\psi(2S) \rightarrow J/\psi\pi^+\pi^-)K^+$ decays, with $J/\psi\pi^+\pi^-$ mass between 3.66 and 3.71 GeV/c^2 . Right: background-subtracted $J/\psi\pi^+\pi^-$ mass distribution from selected B^+ decays. Results of the fits, described in the text, are overlaid.

ment are taken from simulation with the resolution further corrected by a scale factor, $s_{\psi(2S)}$, that accounts for a small discrepancy between data and simulation [26, 102]. To account for the uncertainty in the tail and resolution parameters, the fit is performed simultaneously to data and simulated samples, sharing the same tail parameters, and allowing for the correction factor $s_{\psi(2S)}$ to vary. From this fit the number of $B^+ \rightarrow \psi(2S)K^+$ decays is found to be

$$N_{B^+ \rightarrow \psi(2S)K^+} = (121.40 \pm 0.14) \times 10^3, \quad (3)$$

where the uncertainty is statistical only. The correction factor $s_{\psi(2S)}$ is found to be 1.057 ± 0.008 , which is in good agreement with results from Refs. [15, 26, 97, 98, 102, 103].

6 Branching fraction ratio computation

The ratio of the branching fractions \mathcal{R} , defined in Eq. (1), is calculated as

$$\mathcal{R} = \frac{N_{B^+ \rightarrow J/\psi\eta'K^+}}{N_{B^+ \rightarrow \psi(2S)K^+}} \times \frac{\mathcal{B}(\psi(2S) \rightarrow J/\psi\pi^+\pi^-)}{\mathcal{B}(\eta' \rightarrow \rho^0\gamma)} \times \frac{\epsilon_{B^+ \rightarrow \psi(2S)K^+}}{\epsilon_{B^+ \rightarrow J/\psi\eta'K^+}},$$

where $N_{B^+ \rightarrow J/\psi\eta'K^+}$ and $N_{B^+ \rightarrow \psi(2S)K^+}$ are the yields from Eqs. (2a) and (3), and $\epsilon_{B^+ \rightarrow J/\psi\eta'K^+}$ and $\epsilon_{B^+ \rightarrow \psi(2S)K^+}$ are the efficiencies to reconstruct the observed final states. The efficiencies are the products of detector acceptance, reconstruction, selection and trigger efficiencies, and are calculated using simulated samples, calibrated to match the data as described in Sec. 2. The ratio of branching fractions \mathcal{R} is found to be

$$\frac{\mathcal{B}(B^+ \rightarrow J/\psi\eta'K^+)}{\mathcal{B}(B^+ \rightarrow \psi(2S)K^+)} = (4.91 \pm 0.47) \times 10^{-2},$$

where the uncertainty is statistical only.

As a cross-check, the ratio \mathcal{R} is also calculated for the $\eta' \rightarrow \eta\pi^+\pi^-$, using the signal yields from Eqs. (2b) and (3). The ratio of branching fractions \mathcal{R} is found to be $(4.98 \pm 0.61) \times 10^{-2}$, where the uncertainty is statistical only. This value is in good agreement with that calculated for the $\eta' \rightarrow \rho^0\gamma$ case.

7 Systematic uncertainties

Signal and normalisation channels share the same set of final-state charged particles, and the same trigger and preselection requirements are applied to both. This allows many systematic uncertainties to cancel in the ratio \mathcal{R} . The remaining nonnegligible contributions are listed in Table 1.

A large source of systematic uncertainties is associated to the corrections applied to the simulation. The finite size of the $B^+ \rightarrow J/\psi K^+$ signal sample used for correction of the simulated transverse momentum and rapidity spectra of B^+ mesons induces an uncertainty on the B^+ meson p_T and y spectra. In turn, this uncertainty induces small changes in the ratio of efficiencies. The corresponding spread of these changes amounts to 0.1% and is taken as the systematic uncertainty related to the B^+ meson kinematic.

The decay model corrections for the $B^+ \rightarrow J/\psi \eta' K^+$ decay are obtained using the algorithm described in Ref. [74]. The systematic uncertainty related to the correction method is estimated by varying the configuration parameters of the algorithm. The largest deviation of the efficiency value from the baseline tuning is found to be 1.1%, which is assigned as systematic uncertainty associated with the B^+ decay model.

There are residual differences in the reconstruction efficiency of charged-particle tracks that do not cancel completely in the ratio of total efficiencies given the slightly different kinematic distributions of the final-state particles. The track-finding efficiencies obtained from simulated samples are corrected using calibration channels [76]. The uncertainties related to the efficiency correction factors are propagated to the ratios of the total efficiencies using pseudoexperiments, and are found to be 0.7%. This value is taken as the systematic uncertainty due to the tracking efficiency calibration.

Differences on the photon reconstruction efficiencies between data and simulation are studied using a large sample of $B^+ \rightarrow J/\psi K^{*+}$ decays, reconstructed using the $K^{*+} \rightarrow K^+ (\pi^0 \rightarrow \gamma\gamma)$ decay mode [77–80]. The uncertainty due to the finite size of the sample is propagated to the ratio of the total efficiencies using pseudoexperiments and is found to be less than 1.0%. The uncertainty due to the accuracy of the $B^+ \rightarrow J/\psi K^{*+}$ branching fraction [37] is 3.5%. These two values are added in quadrature to obtain a systematic uncertainty related to the photon reconstruction of 3.6%.

The kaon identification variable used for the MLP estimator is drawn from calibration data samples and has a dependence on the particle kinematics and track multiplicity. Systematic uncertainties in this procedure arise from the limited size of both the simulation and calibration samples, and the modelling of the particle identification variable. The limitations due to the size of the simulation and calibration samples are evaluated by using bootstrapping techniques [104, 105], creating multiple samples and repeating the procedure for each sample. The impact of potential mismodelling of the kaon identification variable is evaluated by describing the corresponding distributions using density estimates with different kernel widths [75, 106]. For each of these cases, alternative efficiency maps are produced to determine the associated uncertainties. A systematic uncertainty of 2.8% is assigned from the observed differences with alternative efficiency maps.

A systematic uncertainty related to the knowledge of the trigger efficiencies has been previously studied using large samples of $B^+ \rightarrow (J/\psi \rightarrow \mu^+ \mu^-) K^+$ and $B^+ \rightarrow (\psi(2S) \rightarrow \mu^+ \mu^-) K^+$ decays by comparing the ratios of the trigger efficiencies in data and simulation [107]. Based on this comparison, a relative uncertainty of 1.1% is assigned.

Table 1: Summary of systematic uncertainties on the ratio of branching fractions \mathcal{R} . The overall systematic uncertainty is calculated as a sum in quadrature of all the sources.

Source	Value [%]
B ⁺ kinematics	0.1
B ⁺ decay model	1.1
Tracking efficiency correction	0.7
Photon reconstruction correction	3.6
Kaon identification	2.8
Trigger efficiency	1.1
Data-simulation agreement	3.0
Fit model	1.6
Simulation sample size	0.9
Total	6.0

The remaining inconsistency between data and simulation, not covered by the corrections discussed in Sec. 2, is estimated by varying the requirement on the response of the MLP classifier in ranges that lead to changes in the measured signal yields as large as $\pm 20\%$. The resulting difference in the data-simulation efficiency ratio is found to be 3.0%.

A different class of systematic uncertainties directly affects the fit itself, namely uncertainties associated to the fit models used to describe the $J/\psi \eta' K^+$, $\psi(2S)K^+$ and $J/\psi \pi^+ \pi^-$ spectra. The systematic uncertainty is accounted for by fits with alternative models. The list of alternative models to describe signal B⁺ and $\psi(2S)$ components includes a modified Apollonios function [108], which has exponential instead of power-law tails, a generalised Student's t -distribution [109, 110] and a modified Novosibirsk function [111]. For the combinatorial background for both the signal and the normalisation channels, a third order polynomial function and an exponential function multiplied by a first order polynomial function are chosen as alternative models. For each fit only one component (either signal or background) is replaced at a time, and the same fit function is used for both signal and normalisation channel. The largest deviation of the ratio of signal yields is found to be 0.6%. As alternative background models for $J/\psi \pi^+ \pi^-$ candidates, a first order polynomial function and a product of an exponential function with a first order polynomial function are used. The largest deviation of the signal yield is found to be 1.5%. The two deviations are added in quadrature to obtain a 1.6% systematic uncertainty due to imperfect knowledge of the signal and background shapes.

Finally, the finite size of the simulation samples contributes an uncertainty of 0.9% on the ratio of total efficiencies. The total systematic uncertainty for the ratio of branching fractions \mathcal{R} is calculated as the sum in quadrature of all the values listed above and is found to be 6.0%.

The statistical significance for the $B^+ \rightarrow J/\psi \eta' K^+$ decay is recalculated using Wilks' theorem for each alternative fit model, and the smallest values of 17 and 10 standard deviations for the $\eta' \rightarrow \rho^0 \gamma$ and $\eta' \rightarrow \eta \pi^+ \pi^-$ cases, respectively, are taken as the significance including the systematic uncertainty.

8 Results and summary

The $B^+ \rightarrow J/\psi\eta'K^+$ decays are observed for the first time using proton-proton collision data collected by the LHCb experiment at centre-of-mass energies of 7, 8, and 13 TeV, corresponding to a total integrated luminosity of 9 fb^{-1} . In the analysis, the η' meson is reconstructed from the two $\rho^0\gamma$ and $\eta\pi^+\pi^-$ final states. The signal significance exceeds 10 standard deviations for both modes. The branching fraction of the $B^+ \rightarrow J/\psi\eta'K^+$ decay is measured for the $\eta' \rightarrow \rho^0\gamma$ sample through normalisation to the known branching fraction of the $B^+ \rightarrow \psi(2S)K^+$ decay [37]. The ratio of branching fractions is found to be

$$\frac{\mathcal{B}(B^+ \rightarrow J/\psi\eta'K^+)}{\mathcal{B}(B^+ \rightarrow \psi(2S)K^+)} = (4.91 \pm 0.47 \pm 0.29 \pm 0.07) \times 10^{-2},$$

where the first uncertainty is statistical, the second is systematic and the third is related to the uncertainties on the branching fractions of the intermediate resonances. The absolute branching fraction is determined using the known branching fraction of $B^+ \rightarrow \psi(2S)K^+$ decays, $\mathcal{B}(B^+ \rightarrow \psi(2S)K^+) = (6.24 \pm 0.20) \times 10^{-4}$ [37], and is found to be

$$\mathcal{B}(B^+ \rightarrow J/\psi\eta'K^+) = (3.06 \pm 0.29 \pm 0.18 \pm 0.04) \times 10^{-5},$$

where the first uncertainty is statistical, the second is systematic and the third is due to external branching fractions uncertainties. An inspection of the $J/\psi\eta'$ mass spectrum shows no significant contributions from the decays via intermediate charmonium or charmonium-like resonances.

References

- [1] Belle collaboration, S. K. Choi *et al.*, *Observation of a narrow charmoniumlike state in exclusive $B^\pm \rightarrow K^\pm \pi^+ \pi^- J/\psi$ decays*, Phys. Rev. Lett. **91** (2003) 262001, arXiv:hep-ex/0309032.
- [2] LHCb collaboration, R. Aaij *et al.*, *Observation of $J/\psi p$ resonances consistent with pentaquark states in $\Lambda_b^0 \rightarrow J/\psi p K^-$ decays*, Phys. Rev. Lett. **115** (2015) 072001, arXiv:1507.03414.
- [3] LHCb collaboration, R. Aaij *et al.*, *Model-independent evidence for $J/\psi p$ contributions to $\Lambda_b^0 \rightarrow J/\psi p K^-$ decays*, Phys. Rev. Lett. **117** (2016) 082002, arXiv:1604.05708.
- [4] LHCb collaboration, R. Aaij *et al.*, *Observation of a narrow pentaquark state, $P_c(4312)^+$, and of two-peak structure of the $P_c(4450)^+$* , Phys. Rev. Lett. **122** (2019) 222001, arXiv:1904.03947.
- [5] LHCb collaboration, R. Aaij *et al.*, *Evidence for exotic hadron contributions to $\Lambda_b^0 \rightarrow J/\psi p \pi^-$ decays*, Phys. Rev. Lett. **117** (2016) 082003, arXiv:1606.06999.
- [6] LHCb collaboration, R. Aaij *et al.*, *Evidence for a new structure in the $J/\psi p$ and $J/\psi \bar{p}$ systems in $B_s^0 \rightarrow J/\psi p \bar{p}$ decays*, Phys. Rev. Lett. **128** (2022) 062001, arXiv:2108.04720.
- [7] LHCb collaboration, R. Aaij *et al.*, *Evidence of a $J/\psi \Lambda$ structure and observation of excited Ξ^- states in the $\Xi_b^- \rightarrow J/\psi \Lambda K^-$ decay*, Science Bulletin **66** (2021) 1278, arXiv:2012.10380.
- [8] Belle collaboration, S. K. Choi *et al.*, *Observation of a resonance-like structure in the $\pi^\pm \psi'$ mass distribution in exclusive $B \rightarrow K \pi^\pm \psi'$ decays*, Phys. Rev. Lett. **100** (2008) 142001, arXiv:0708.1790.
- [9] Belle collaboration, R. Mizuk *et al.*, *Dalitz analysis of $B \rightarrow K \pi^+ \psi'$ decays and the $Z(4430)^+$* , Phys. Rev. **D80** (2009) 031104, arXiv:0905.2869.
- [10] Belle collaboration, K. Chilikin *et al.*, *Experimental constraints on the spin and parity of the $Z(4430)^+$* , Phys. Rev. **D88** (2013) 074026, arXiv:1306.4894.
- [11] LHCb collaboration, R. Aaij *et al.*, *Observation of the resonant character of the $Z(4430)^-$ state*, Phys. Rev. Lett. **112** (2014) 222002, arXiv:1404.1903.
- [12] LHCb collaboration, R. Aaij *et al.*, *Model-independent confirmation of the $Z(4430)^-$ state*, Phys. Rev. **D92** (2015) 112009, arXiv:1510.01951.
- [13] LHCb collaboration, R. Aaij *et al.*, *Observation of exotic $J/\psi \phi$ structures from amplitude analysis of $B^+ \rightarrow J/\psi \phi K^+$ decays*, Phys. Rev. Lett. **118** (2017) 022003, arXiv:1606.07895.
- [14] LHCb collaboration, R. Aaij *et al.*, *Amplitude analysis of $B^+ \rightarrow J/\psi \phi K^+$ decays*, Phys. Rev. **D95** (2017) 012002, arXiv:1606.07898.

- [15] LHCb collaboration, R. Aaij *et al.*, *Study of $B_s^0 \rightarrow J/\psi \pi^+ \pi^- K^+ K^-$ decays*, JHEP **02** (2021) 024, [arXiv:2011.01867](#).
- [16] LHCb collaboration, R. Aaij *et al.*, *Observation of new resonances decaying to $J/\psi K^+$ and $J/\psi \phi$* , Phys. Rev. Lett. **127** (2021) 082001, [arXiv:2103.01803](#).
- [17] LHCb collaboration, R. Aaij *et al.*, *Evidence of a $J/\psi K_S^0$ structure in $B^0 \rightarrow J/\psi \phi K_S^0$ decays*, [arXiv:2301.04899](#), submitted to Phys. Rev. Lett.
- [18] LHCb collaboration, R. Aaij *et al.*, *Evidence for a $\eta_c(1S)\pi^-$ resonance in $B^0 \rightarrow \eta_c(1S)K^+\pi^-$ decays*, Eur. Phys. J. **C78** (2018) 1019, [arXiv:1809.07416](#).
- [19] LHCb collaboration, R. Aaij *et al.*, *Model-independent observation of exotic contributions to $B^0 \rightarrow J/\psi K^+\pi^-$ decays*, Phys. Rev. Lett. **122** (2019) 152002, [arXiv:1901.05745](#).
- [20] LHCb collaboration, R. Aaij *et al.*, *Observation of $B_s^0 \rightarrow \chi_{c1} \phi$ decay and study of $B^0 \rightarrow \chi_{c1,2} K^{*0}$ decays*, Nucl. Phys. **B874** (2013) 663, [arXiv:1305.6511](#).
- [21] LHCb collaboration, R. Aaij *et al.*, *Evidence for the decay $X(3872) \rightarrow \psi(2S)\gamma$* , Nucl. Phys. **B886** (2014) 665, [arXiv:1404.0275](#).
- [22] LHCb collaboration, R. Aaij *et al.*, *Observation of the decays $\Lambda_b^0 \rightarrow \chi_{c1} p K^-$ and $\Lambda_b^0 \rightarrow \chi_{c2} p K^-$* , Phys. Rev. Lett. **119** (2017) 062001, [arXiv:1704.07900](#).
- [23] LHCb collaboration, R. Aaij *et al.*, *Observation of the decay $\Lambda_b^0 \rightarrow \chi_{c1} p \pi^-$* , JHEP **05** (2021) 095, [arXiv:2103.04949](#).
- [24] LHCb collaboration, R. Aaij *et al.*, *Determination of the $X(3872)$ meson quantum numbers*, Phys. Rev. Lett. **110** (2013) 222001, [arXiv:1302.6269](#).
- [25] LHCb collaboration, R. Aaij *et al.*, *Quantum numbers of the $X(3872)$ state and orbital angular momentum in its $\rho^0 J/\psi$ decays*, Phys. Rev. **D92** (2015) 011102(R), [arXiv:1504.06339](#).
- [26] LHCb collaboration, R. Aaij *et al.*, *Study of the $\psi_2(3823)$ and $\chi_{c1}(3872)$ states in $B^+ \rightarrow (J/\psi \pi^+ \pi^-) K^+$ decays*, JHEP **08** (2020) 123, [arXiv:2005.13422](#).
- [27] LHCb collaboration, R. Aaij *et al.*, *Observation of sizeable ω contribution to $\chi_{c1}(3872) \rightarrow \pi^+ \pi^- J/\psi$ decays*, [arXiv:2204.12597](#), to appear in Phys. Rev. D.
- [28] BaBar collaboration, P. del Amo Sanchez *et al.*, *Evidence for the decay $X(3872) \rightarrow J/\psi \omega$* , Phys. Rev. **D82** (2010) 011101, [arXiv:1005.5190](#).
- [29] LHCb collaboration, R. Aaij *et al.*, *Study of charmonium and charmonium-like contributions in $B^+ \rightarrow J/\psi \eta K^+$ decays*, JHEP **04** (2021) 46, [arXiv:2202.04045](#).
- [30] Belle collaboration, X. L. Wang *et al.*, *Observation of $\psi(4040)$ and $\psi(4160)$ decay into $\eta J/\psi$* , Phys. Rev. D **87** (2013) 051101, [arXiv:1210.7550](#).
- [31] BES III collaboration, M. Ablikim *et al.*, *Observation of the $Y(4220)$ and $Y(4360)$ in the process $e^+e^- \rightarrow \eta J/\psi$* , Phys. Rev. D **102** (2020) 031101, [arXiv:2003.03705](#).

- [32] N. Brambilla *et al.*, *The XYZ states: experimental and theoretical status and perspectives*, Phys. Rept. **873** (2020) 1, [arXiv:1907.07583](#).
- [33] A. Ali, L. Maiani, and A. D. Polosa, *Multiquark hadrons*, Cambridge University Press, 2019.
- [34] L. Maiani and A. Pilloni, *GGI Lectures on exotic hadrons*, 2022, [arXiv:2207.05141](#).
- [35] N. Brambilla *et al.*, *Substructure of multiquark hadrons (Snowmass 2021 White Paper)*, [arXiv:2203.16583](#).
- [36] N. Brambilla *et al.*, *Heavy Quarkonium: progress, puzzles, and opportunities*, Eur. Phys. J. **C71** (2011) 1534, [arXiv:1010.5827](#).
- [37] Particle Data Group, R. L. Workman *et al.*, *Review of particle physics*, Prog. Theor. Exp. Phys. **2022** (2022) 083C01.
- [38] J. L. Rosner, *Quark content of neutral mesons*, Phys. Rev. **D27** (1983) 1101.
- [39] A. Bramon, R. Escribano, and M. D. Scadron, *The $\eta - \eta'$ mixing angle revisited*, Eur. Phys. J. **C7** (1999) 271, [arXiv:hep-ph/9711229](#).
- [40] A. Bramon, R. Escribano, and M. D. Scadron, *Mixing of $\eta - \eta'$ mesons in J/ψ decays into a vector and a pseudoscalar meson*, Phys. Lett. **B403** (1997) 339, [arXiv:hep-ph/9703313](#).
- [41] V. A. Novikov, M. A. Shifman, A. I. Vainshtein, and V. I. Zakharov, *A theory of the $J/\psi \rightarrow \eta(\eta')\gamma$ decays*, Nucl. Phys. **B165** (1980) 55.
- [42] V. A. Novikov, M. A. Shifman, A. I. Vainshtein, and V. I. Zakharov, *η' meson as pseudoscalar gluonium*, Phys. Lett. **B86** (1979) 347.
- [43] V. A. Novikov, M. A. Shifman, A. I. Vainshtein, and V. I. Zakharov, *In a search for scalar gluonium*, Nucl. Phys. **B165** (1980) 67.
- [44] A. L. Kataev, N. V. Krasnikov, and A. A. Pivovarov, *The connection between the scales of the gluon and quark worlds in perturbative QCD*, Phys. Lett. **B107** (1981) 115.
- [45] A. L. Kataev, N. V. Krasnikov, and A. A. Pivovarov, *Two loop calculations for the propagators of gluonic currents*, Nucl. Phys. **B198** (1982) 508, [arXiv:hep-ph/9612326](#).
- [46] C. E. Thomas, *Composition of the pseudoscalar η and η' mesons*, JHEP **10** (2007) 026, [arXiv:0705.1500](#).
- [47] R. Escribano and J. Nadal, *On the gluon content of the η and η' mesons*, JHEP **05** (2007) 006, [arXiv:hep-ph/0703187](#).
- [48] R. Escribano, *$J/\psi \rightarrow VP$ decays and the quark and gluon content of the η and η'* , Eur. Phys. J. **C65** (2010) 467, [arXiv:0807.4201](#).

- [49] F. Ambrosino *et al.*, *A global fit to determine the pseudoscalar mixing angle and the gluonium content of the η' meson*, JHEP **07** (2009) 105, arXiv:0906.3819.
- [50] CLEO collaboration, J. Yelton *et al.*, *Absolute branching fraction measurements for exclusive $D_{(s)}$ semileptonic decays*, Phys. Rev. **D80** (2009) 052007, arXiv:0903.0601.
- [51] CLEO collaboration, J. Yelton *et al.*, *Studies of $D^+ \rightarrow (\eta', \eta, \phi) e^+ \nu_e$* , Phys. Rev. **D84** (2011) 032001, arXiv:1011.1195.
- [52] C. Di Donato, G. Ricciardi, and I. Bigi, *$\eta - \eta'$ mixing – from electromagnetic transitions to weak decays of charm and beauty hadrons*, Phys. Rev. **D85** (2012) 013016, arXiv:1105.3557.
- [53] LHCb collaboration, R. Aaij *et al.*, *Study of $\eta - \eta'$ mixing from measurement of $B_{(s)}^0 \rightarrow J/\psi \eta^{(\prime)}$ decay rates*, JHEP **01** (2015) 024, arXiv:1411.0943.
- [54] M. A. Andreichikov, M. I. Vysotsky, and V. A. Novikov, *On the branching ratios of the $B^0 \rightarrow J/\psi \eta (\eta', \pi^0)$ and $B_s^0 \rightarrow J/\psi \eta (\eta')$ decays*, Pisma Zh. Eksp. Teor. Fiz. **110** (2019) 633.
- [55] M. A. Andreichikov, M. I. Eides, V. A. Novikov, and M. I. Vysotsky, *The physics of the $\eta - \eta'$ system versus $B^0 \rightarrow J/\psi \eta (\eta')$ and $B_s^0 \rightarrow J/\psi \eta (\eta')$ decays*, Int. J. Mod. Phys. **A35** (2020) 2050111, arXiv:1911.10596.
- [56] F. E. Close *et al.*, *Gluonic hadrons and charmless B decays*, Phys. Rev. **D57** (1998) 5653, arXiv:hep-ph/9708265.
- [57] F. E. Close and P. R. Page, *Gluonic charmonium resonances at BaBar and Belle?*, Phys. Lett. **B628** (2005) 215, arXiv:hep-ph/0507199.
- [58] Belle collaboration, Q. L. Xie *et al.*, *Search for $B^+ \rightarrow J/\psi \eta' K^+$ and $B^0 \rightarrow J/\psi \eta' K_S^0$ decays*, Phys. Rev. **D75** (2007) 017101, arXiv:hep-ex/0610084.
- [59] LHCb collaboration, A. A. Alves Jr. *et al.*, *The LHCb detector at the LHC*, JINST **3** (2008) S08005.
- [60] LHCb collaboration, R. Aaij *et al.*, *LHCb detector performance*, Int. J. Mod. Phys. **A30** (2015) 1530022, arXiv:1412.6352.
- [61] R. Aaij *et al.*, *Performance of the LHCb Vertex Locator*, JINST **9** (2014) P09007, arXiv:1405.7808.
- [62] R. Arink *et al.*, *Performance of the LHCb Outer Tracker*, JINST **9** (2014) P01002, arXiv:1311.3893.
- [63] P. d'Argent *et al.*, *Improved performance of the LHCb Outer Tracker in LHC Run 2*, JINST **12** (2017) P11016, arXiv:1708.00819.
- [64] M. Adinolfi *et al.*, *Performance of the LHCb RICH detector at the LHC*, Eur. Phys. J. **C73** (2013) 2431, arXiv:1211.6759.

- [65] A. A. Alves Jr. *et al.*, *Performance of the LHCb muon system*, JINST **8** (2013) P02022, [arXiv:1211.1346](#).
- [66] R. Aaij *et al.*, *The LHCb trigger and its performance in 2011*, JINST **8** (2013) P04022, [arXiv:1211.3055](#).
- [67] R. Aaij *et al.*, *Performance of the LHCb trigger and full real-time reconstruction in Run 2 of the LHC*, JINST **14** (2019) P04013, [arXiv:1812.10790](#).
- [68] T. Sjöstrand, S. Mrenna, and P. Skands, *A brief introduction to PYTHIA 8.1*, Comput. Phys. Commun. **178** (2008) 852, [arXiv:0710.3820](#).
- [69] I. Belyaev *et al.*, *Handling of the generation of primary events in GAUSS, the LHCb simulation framework*, J. Phys. Conf. Ser. **331** (2011) 032047.
- [70] D. J. Lange, *The EVTGEN particle decay simulation package*, Nucl. Instrum. Meth. **A462** (2001) 152.
- [71] N. Davidson, T. Przedzinski, and Z. Was, *PHOTOS interface in C++: Technical and physics documentation*, Comp. Phys. Comm. **199** (2016) 86, [arXiv:1011.0937](#).
- [72] Geant4 collaboration, J. Allison *et al.*, *GEANT4 developments and applications*, IEEE Trans. Nucl. Sci. **53** (2006) 270; Geant4 collaboration, S. Agostinelli *et al.*, *GEANT4: A simulation toolkit*, Nucl. Instrum. Meth. **A506** (2003) 250.
- [73] M. Clemencic *et al.*, *The LHCb simulation application, GAUSS: Design, evolution and experience*, J. Phys. Conf. Ser. **331** (2011) 032023.
- [74] A. Rogozhnikov, *Reweighting with boosted decision trees*, J. Phys. Conf. Ser. **762** (2016) 012036, [arXiv:1608.05806](#), https://github.com/arogozhnikov/hep_ml.
- [75] R. Aaij *et al.*, *Selection and processing of calibration samples to measure the particle identification performance of the LHCb experiment in Run 2*, Eur. Phys. J. Tech. Instr. **6** (2019) 1, [arXiv:1803.00824](#).
- [76] LHCb collaboration, R. Aaij *et al.*, *Measurement of the track reconstruction efficiency at LHCb*, JINST **10** (2015) P02007, [arXiv:1408.1251](#).
- [77] LHCb collaboration, R. Aaij *et al.*, *Evidence for the decay $B^0 \rightarrow J/\psi\omega$ and measurement of the relative branching fractions of B_s^0 meson decays to $J/\psi\eta$ and $J/\psi\eta'$* , Nucl. Phys. **B867** (2013) 547, [arXiv:1210.2631](#).
- [78] LHCb collaboration, R. Aaij *et al.*, *Observations of $B_s^0 \rightarrow \psi(2S)\eta$ and $B_{(s)}^0 \rightarrow \psi(2S)\pi^+\pi^-$ decays*, Nucl. Phys. **B871** (2013) 403, [arXiv:1302.6354](#).
- [79] E. Govorkova, *Study of π^0/γ efficiency using B meson decays in the LHCb experiment*, Phys. Atom. Nucl. **79** (2016) 1474, [arXiv:1505.02960](#).
- [80] K. Govorkova, *Study of photons and neutral pions reconstruction efficiency in the LHCb experiment*, Master thesis, Lomonosov Moscow State University, Moscow, Russia, 2015, CERN-THESIS-2015-272.

- [81] A. Powell *et al.*, *Particle identification at LHCb*, PoS **ICHEP2010** (2010) 020, LHCb-PROC-2011-008.
- [82] H. Terrier and I. Belyaev, *Particle identification with LHCb calorimeters*, LHCb-2003-092, 2003.
- [83] C. Abellan Beteta *et al.*, *Calibration and performance of the LHCb calorimeters in Run 1 and 2 at the LHC*, arXiv:2008.11556, submitted to JINST.
- [84] TASSO collaboration, M. Althoff *et al.*, *Measurement of the radiative width of the $\eta'(958)$ in two-photon interactions*, Phys. Lett. **B147** (1984) 487.
- [85] H. Kolanoski, *Two-photon physics at e^+e^- storage rings*, vol. 105, Berlin, Springer-Verlag, 1984.
- [86] ARGUS collaboration, H. Albrecht *et al.*, *Observation of the decay $D_s^+ \rightarrow \eta'\pi^+$* , Phys. Lett. **B245** (1990) 315.
- [87] CLEO collaboration, M. Daoudi *et al.*, *Two-body D_s^+ decays to $\eta\pi^+$, $\eta'\pi^+$, $\eta\rho^+$, $\eta'\rho^+$ and $\phi\rho^+$* , Phys. Rev. **D45** (1992) 3965.
- [88] CLEO collaboration, J. P. Alexander *et al.*, *D_s^+ decays to $\eta\pi^+$ and $\eta'\pi^+$* , Phys. Rev. Lett. **68** (1992) 1275.
- [89] BESIII collaboration, M. Ablikim *et al.*, *Precision study of $\eta' \rightarrow \gamma\pi^+\pi^-$ decay dynamics*, Phys. Rev. Lett. **120** (2018) 242003, arXiv:1712.01525.
- [90] W. D. Hulsbergen, *Decay chain fitting with a Kalman filter*, Nucl. Instrum. Meth. **A552** (2005) 566, arXiv:physics/0503191.
- [91] W. S. McCulloch and W. Pitts, *A logical calculus of the ideas immanent in nervous activity*, The bulletin of mathematical biophysics **5** (1943) 115.
- [92] F. Rosenblatt, *The perceptron: A probabilistic model for information storage and organization in the brain*, Psychological Review **65** (1958) 386.
- [93] J.-H. Zhong *et al.*, *A program for the Bayesian neural network in the ROOT framework*, Comput. Phys. Commun. **182** (2011) 2655, arXiv:1103.2854.
- [94] T. Skwarnicki, *A study of the radiative cascade transitions between the Υ' and Υ resonances*, PhD thesis, Institute of Nuclear Physics, Krakow, 1986, DESY-F31-86-02.
- [95] LHCb collaboration, R. Aaij *et al.*, *Observation of J/ψ -pair production in pp collisions at $\sqrt{s} = 7$ TeV*, Phys. Lett. **B707** (2012) 52, arXiv:1109.0963.
- [96] S. Karlin and L. S. Shapley, *Geometry of moment spaces*, vol. 12 of *Memoirs of the American Mathematical Society*, American Mathematical Society, Providence, Rhode Island, 1953.
- [97] LHCb collaboration, R. Aaij *et al.*, *Study of B_c^+ decays to charmonia and three light hadrons*, JHEP **01** (2022) 065, arXiv:2111.03001.

- [98] LHCb collaboration, R. Aaij *et al.*, *Study of B_c^+ decays to charmonia plus multihadron final states*, arXiv:2208.08660, to appear in JHEP.
- [99] S. S. Wilks, *The large-sample distribution of the likelihood ratio for testing composite hypotheses*, Ann. Math. Stat. **9** (1938) 60.
- [100] M. Pivk and F. R. Le Diberder, *sPlot: A statistical tool to unfold data distributions*, Nucl. Instrum. Meth. **A555** (2005) 356, arXiv:physics/0402083.
- [101] E. Byckling and K. Kajantie, *Particle kinematics*, John Wiley & Sons Inc., New York, 1973.
- [102] LHCb collaboration, R. Aaij *et al.*, *Study of the line shape of the $\chi_{c1}(3872)$ state*, Phys. Rev. **D102** (2020) 092005, arXiv:2005.13419.
- [103] LHCb collaboration, R. Aaij *et al.*, *Observation of the $B_s^0 \rightarrow \chi_{c1}(3872)\pi^+\pi^-$ decay*, arXiv:2302.10629, submitted to JHEP.
- [104] B. Efron, *Bootstrap methods: Another look at the jackknife*, Ann. Statist. **7** (1979) 1.
- [105] B. Efron and R. J. Tibshirani, *An introduction to the bootstrap*, Chapman and Hall, New York, 1994.
- [106] A. Poluektov, *Kernel density estimation of a multidimensional efficiency profile*, JINST **10** (2015) P02011, arXiv:1411.5528.
- [107] LHCb collaboration, R. Aaij *et al.*, *Measurement of relative branching fractions of B decays to $\psi(2S)$ and J/ψ mesons*, Eur. Phys. J. **C72** (2012) 2118, arXiv:1205.0918.
- [108] D. Martínez Santos and F. Dupertuis, *Mass distributions marginalized over per-event errors*, Nucl. Instrum. Meth. **A764** (2014) 150, arXiv:1312.5000.
- [109] Student (W. S. Gosset), *The probable error of a mean*, Biometrika **6** (1908) 1.
- [110] S. Jackman, *Bayesian analysis for the social sciences*, John Wiley & Sons, Inc., Hoboken, New Jersey, USA, 2009.
- [111] BaBar collaboration, J. P. Lees *et al.*, *Branching fraction measurements of the color-suppressed decays $\bar{B}^0 \rightarrow D^{(*)0}\pi^0$, $D^{(*)0}\eta$, $D^{(*)0}\omega$, and $D^{(*)0}\eta'$ and measurement of the polarization in the decay $\bar{B}^0 \rightarrow D^{*0}\omega$* , Phys. Rev. **D84** (2011) 112007, Erratum ibid. **D87** (2013) 039901, arXiv:1107.5751.